Published in final edited form as:

J Cell Physiol. 2018 February ; 233(2): 1156–1167. doi:10.1002/jcp.25976.

The Skeletal Cell-Derived Molecule Sclerostin Drives Bone Marrow Adipogenesis

Heather Fairfield[1,2,3], **Carolyne Falank**[1,2,3], **Elizabeth Harris**[1,2,3], **Victoria Demambro**[1,2,3], **Michelle McDonald**[4], **Jessica A Pettit**[4], **Sindhu T Mohanty**[4], **Peter Croucher**[4], **Ina Kramer**[5], **Michaela Kneissel**[5], **Clifford J. Rosen**[1,2,3], and **Michaela R. Reagan**[1,2,3]

[1]Center for Clinical and Translational Research, Maine Medical Center Research Institute, Scarborough, ME, USA [2]University of Maine Graduate School of Biomedical Science and Engineering, Orono, ME, USA [3]Tufts University School of Medicine, Boston, MA, USA [4]The Garvan Institute of Medical Research, Sydney, NSW, Australia [5]Novartis Institutes for BioMedical Research, Basel, Switzerland

Abstract

The bone marrow niche is a dynamic and complex microenvironment that can both regulate, and be regulated by the bone matrix. Within the bone marrow (BM), mesenchymal stromal cell (MSC) precursors reside in a multi-potent state and retain the capacity to differentiate down osteoblastic, adipogenic, or chondrogenic lineages in response to numerous biochemical cues. These signals can be altered in various pathological states including, but not limited to, osteoporotic-induced fracture, systemic adiposity, and the presence of bone-homing cancers. Herein we provide evidence that signals from the bone matrix (osteocytes) determine marrow adiposity by regulating adipogenesis in the bone marrow. Specifically, we found that physiologically relevant levels of Sclerostin (SOST), which is a Wnt-inhibitory molecule secreted from bone matrix-embedded osteocytes, can induce adipogenesis in 3T3-L1 cells, mouse ear- and BM-derived MSCs, and human BM-derived MSCs. We demonstrate that the mechanism of SOST induction of adipogenesis is through inhibition of Wnt signaling in pre-adipocytes. We also demonstrate that a decrease of sclerostin *in vivo*, via both genetic and pharmaceutical methods, significantly decreases bone marrow adipose tissue (BMAT) formation. Overall, this work demonstrates a direct role for SOST in regulating fate determination of BM-adipocyte progenitors. This provides a novel mechanism for which BMAT is governed by the local bone microenvironment, which may prove relevant in the pathogenesis of certain diseases involving marrow adipose. Importantly, with anti-sclerostin therapy at the forefront of osteoporosis treatment and a greater recognition of the role of BMAT in disease, these data are likely to have important clinical implications.

Corresponding Author and person to whom reprint requests should be addressed: Michaela R. Reagan, PhD, Center for Molecular Medicine and Center for Translational Research, 81 Research Drive, Scarborough, Maine. USA 04074, Phone: 1-207-396-8196.

Conflicts of Interest for this work: Michaela Kneissel and Ina Kramer are employees of Novartis Pharma. The other authors have no conflicts of interest.

Keywords

Bone Marrow Adipose; Sclerostin; Bone Marrow Microenvironment; Osteocyte-derived factors

Introduction

The bone marrow (BM) niche contains stem, progenitor, and differentiated cell types of several hematopoietic and mesenchymal lineages that cooperate to maintain a complex microenvironment influenced by endocrine, paracrine, and autocrine factors. In the BM, mesenchymal stromal cells (MSCs) differentiate into either adipocytes or osteoblasts in response to an array of factors, some of which are well-known and others are incompletely defined. Understanding how MSCs decide which lineage pathway to follow is crucial in understanding the origins of bone marrow adipose tissue (BMAT), a unique adipose depot that has been newly identified as an important endocrine tissue. BMAT has different responsive phenotypes compared to white adipose tissue (WAT) or brown adipose tissue (BAT), and may play a role in diseases such as osteoporosis and bone metastasis (Falank et al. 2016; Scheller & Rosen 2014). BMAT is elevated in aging, menopause, anorexia nervosa, drug (rosiglitazone) treatment, or high fat diet conditions (Hardouin et al. 2016; Doucette et al. 2015). Interestingly, often high BMAT correlates with low bone mass or osteoblast activity/number, indicating that the decision for MSCs to differentiate into an osteoblast or adipocyte can create a tug-of-war between BMAT and bone tissue. Moreover, recent MSC engraftment experiments with young and aged mice found decreased osteoblastogenesis and increased adipogenesis from MSCs from young mice transplanted into old mice versus transplanted into young mice, demonstrating the importance of the BM microenvironment in determining MSC lineage commitment (Singh et al. 2016). Together these reports demonstrate the importance of bone-derived signals on energy metabolism and BM adipogenesis. As we begin to understand how BMAT plays a role in disease pathologies, it is becoming clear that a better understanding of the molecules that govern BM adipogenesis is needed.

Osteocytes are the most abundant cell type in the bone and have been called the “Master Orchestrators” (Schaffler et al. 2014) of due to their key roles in signaling and mechano/chemical-sensing. We hypothesized that osteocytes regulate the lineage pathway decisions of MSCs within the local BM microenvironment that determine BM adipocyte or osteoblast development. Specifically, we hypothesized that osteocytes secrete factors that trigger responses in BMAT precursors, similarly to how osteocytes modify other effector cells including osteoblasts and osteoclasts through paracrine signaling. Interestingly, despite their integral role in bone homeostasis, osteocytes have not been explored previously for their ability to influence BM adipogenesis.

Unlike the relationship between bone cells and BMAT, which is still poorly understood, the relationship between bone or bone-derived signals and peripheral adipose depots has been investigated previously. Osteolineage cells have been shown to influence global energy metabolism in a number of studies which specifically highlight osteoblast- and osteocyte-derived osteocalcin as a regulator of insulin sensitivity and secretion, and white adipogenesis

(Fulzele et al. 2010). Similar studies also demonstrate that osteocalcin is not the only bone-derived hormone able to influence white adipose tissue and energy expenditure (Yoshikawa et al. 2011). In addition to osteocalcin, lipocalin is a newly identified bone-derived factor that regulates appetite, body weight, and white adipose depots through signaling in the hypothalamus (Mosialou et al. 2017). Thus, bone is known to be a signaling organ that secretes factors to regulate distant adipose depots; however, the effect of bone and bone-derived factors on BM adipose specifically has not been previously defined. Herein we propose a novel concept of a paracrine signaling loop connecting bone and bone marrow adipose. We explored if bone-derived factors could signal between bone and bone marrow cells to maintain homeostasis and bone health. Specifically, we theorized that osteocytes determine a balance between cell types through secretion of proteins that induce bone marrow adipose and inhibit bone formation. If bone cells directly regulate BMAT, as examined here, and BMAT regulates bone mass accrual, as research suggests (Scheller & Rosen 2014; de Paula et al. 2015; Shen et al. 2014), then bone and BMAT are intimately connected via a feedback loop not previously appreciated. In sum, our work contributes to identifying and characterizing the major biochemical mediators regulating the paracrine loop that maintains equilibrium in the bone marrow.

Sclerostin, a Wnt inhibitor encoded by the gene *SOST*, is an osteocyte-derived molecule that holds potential as the candidate signal protein communicating from bone to adipose. Sclerostin has long been associated with bone disease; in humans, inactivating mutations in *Sost* cause Van Buchem disease or sclerosteosis, two genetic conditions characterized by high bone mass (Tian et al. 2011; Li et al. 2011). Sclerostin knockout mice display high bone mass due to increased bone formation (Li et al. 2008), as well as increased callus mass and enhanced strength during fracture healing (Li et al. 2011). In mechanical loading, the downregulation of *Sost*/sclerostin in osteocytes has been found to be an obligatory step in the mechanotransduction cascade that activates Wnt signaling, osteogenesis, and bone-building (Tu et al. 2012). Interestingly, anti-sclerostin antibodies have been shown to stimulate bone formation and inhibit bone resorption in animal models of osteogenesis imperfecta (Roschger et al. 2014), osteoporosis (Ominsky et al. 2017; Li et al. 2014), fracture repair (Florio et al. 2016) and mechanical unloading (Tian et al. 2011). Sclerostin-neutralizing antibodies have been found to transform bone lining mesenchymal stromal cells into active osteoblasts through inhibition of the internalization of sclerostin and sclerostin-mediated antagonism of Wnt signaling through Lrp6 (Kim et al. 2016; van Dinther et al. 2013). In the osteoblast and pre-osteoblast, Wnt signaling leads to the expression of T-cell factor/lymphoid-enhancer (*Tcf/Lef*) family transcription factors, which enhance RUNX2 and other osteogenic genes that induce osteoblast differentiation and proliferation (Heath et al. 2009). Activation of canonical Wnt signaling also inhibits apoptosis in osteoblast-lineage cells (Almeida et al. 2005). In white adipose, which is known to be different from BMAT in many ways, Wnt signaling has also been shown to inhibit adipogenesis and transcription of adipocyte-specific genes including PPARγ through both β-catenin dependent and independent pathways (Kennell & MacDougald 2005; Ukita et al. 2016; Gustafson & Smith 2012), but this signaling pathway, and the role of SOST specifically, in BMAT adipogenesis is largely unknown. Interestingly, parathyroid hormone (PTH) administration has been shown to suppress BMAT, and conditional deletion of PTH1R using the Prx1Cre

recombinase results in a substantial increase in BMAT (Fan et al. 2017). In addition to PTH's stimulation of osteogenesis, PTH also inhibits Sost by acting on the parathyroid hormone (PTH)/PTH-related peptide type 1 receptor (PPR) in osteocytes (Saini et al. 2013; Keller & Kneissel 2005). Thus, PTH may reduce BMAT development in part through its inhibition of sclerostin expression and signaling. Still, it remains unknown if sclerostin can induce marrow adipogenesis directly and if inhibition of sclerostin inhibits this process. If so, targeting sclerostin to modify BM adipose may be a secondary mechanism of action for anti-sclerostin antibodies that are already in clinical trials and showing promising results for patients with osteoporosis (McClung et al. 2014; Genant et al. 2017; Costa et al. 2014).

Materials and Methods

Animals and *In Vivo* Experiments

All animal experiments were performed in accordance with an approved protocol of the Garvan Institute/St. Vincent's Hospital Animal Ethics committee (Sydney, Australia) and the Maine Medical Center Research Ethics Committee (Scarborough, ME). All mice were fed a diet of normal chow and autoclaved water. Osteocalcin-driven yellow fluorescent protein (YFP-OCN) expressing mice were donated from Dr. David Scadden's laboratory (Harvard University Department of Stem Cell & Regenerative Biology, Cambridge, MA). Sost-knockout (SOST-KO) and C57BL/KaLwRijHsd mice were housed and bred in the Garvin Institute. YFP-OCN mice were maintained as YFP+ × YFP+ and housed and bred at Maine Medical Center Research Institute (MMCRI). C57BL/6J mice were purchased from The Jackson Laboratory (Bar Harbor, ME) and bred at the MMCRI. All mice were weaned at 21 days after birth and fed standard chow containing 4% fat. Six-week-old C57BL/KaLwRijHsd male mice were treated weekly with vehicle buffer or Anti-Scl (i.v. 100mg/kg, Novartis Pharma) for 3 weeks and then sacrificed for analysis. Sost-KO and WT male mice were sacrificed at 5–6 weeks old for BMAT analysis.

Cell Line Cultures

3T3-L1 cells were obtained from the ATCC and grown to confluence in Dulbecco's modified Eagle's medium (DMEM, Corning Inc, Corning, NY) with 1% penicillin-streptomycin (GIBCO, Grand Island, NY) at 37°C in a humidified atmosphere of 5% CO_2. For adipocyte differentiation, at two days post-confluence (day 0), differentiation was induced using 500 μM 3-isobutyl-1-methylxanthine (IBMX), 5 μg/mL insulin, 1 μM dexamethasone added to basal media. At day 4, medium was replaced with adipogenic medium containing DMEM supplemented with 10% FBS and 10 μg/mL insulin, which was changed every two days (Morrison & Farmer 1999). All cell culture reagents were from VWR unless otherwise noted.

Primary Cell Cultures

Mouse bone marrow-derived MSC (BM-MSC) cultures were obtained as described previously (Urs et al. 2010). Briefly, tibia and femur were dissected from YFP-OCN or WT C57BL/6J male and female mice. The bones were cleaned, the ends were cut off, and bones were centrifuged at 3,000 rpm for five minutes to isolate BM into 1.5 mL microcentrifuge tubes. This BM was resuspended into DMEM supplemented with 10% FBS and 1%

antibiotic-antimycotic and directly seeded onto a T75 flask and expanded for later use. Mouse BM-MSCs were differentiated into adipocytes using an induction media consisting basal media supplemented with 0.5mM IBMX, 1 μM rosiglitazone, 1 μM dexamethasone, 10 μg/mL insulin once MSCs were 50–70% confluent (day 0). This media was used at day 0 and day 2, and changed to basal media supplemented with 10 μg/mL insulin and 1 μM Rosiglitazone at day 4 and then maintained in basal media supplemented with 10 μg/mL insulin at day 7 and thereafter.

Primary osteocytes were extracted using a published method (Stern et al. 2012). Tibia and femur were dissected and isolated from C57BL/6J or YFP-OCN mice, and bone was sliced into small pieces using a scalpel and/or razor blade prior to sequential digestions with Collagenase I (200 U/mL, Alfa Aesar, Ward Hill, MA). Osteocytes were seeded on collagen-coated cell culture plates (BIOCOAT, Corning Inc, Corning, NY) and maintained in a basal media consisting of αMEM supplemented with 5% FBS, 5% calf serum and 1% antibiotic-antimycotic.

Osteocyte-conditioned Media

Osteocyte conditioned media was made by culturing primary osteocytes (10–12 days after isolation) in fresh basal osteocyte media for 2 days, and removing and centrifuging media at 1200 rcf for 5 minutes to purify media. Control media was identical but without preconditioning from osteocytes. A 50/50 mix of fresh adipogenic media created in an αMEM basal media and osteocyte-conditioned media were used for osteocyte conditioned media experiments.

Mouse ear tissue MSCs were isolated from C57BL/6J mice, and cultured and differentiated as previously described (Liaw et al. 2016). Primary human BM-MSCs were isolated from deidentified cancellous bone from the acetabulum received from donors (men and women) after total hip arthroplasty through the MMCRI Biobank after IRB approval and informed consent. Human BM-MSCs were isolated by surface adherence and cultured as previously described (Reagan et al. 2014; Schutze et al. 2005) with a growth media of DMEM, 10% FBS and 1% antibiotic-antimycotic. Cells were differentiated in adipogenic media consisting of HAMS F12/DMEM with 10% FBS and 1% antibiotic -antimycotic supplemented with 0.5mM 3-isobutyl-1-methylxanthine (IBMX), 0.05 mM indomethacin, 1 μM dexamethasone, and 1 μM insulin.

Histology

Mouse legs were fixed in 10% neutral buffered formalin (NBF) and decalcified in 0.34M EDTA (pH 8.0) solution until soft. Bones were then paraffin embedded, sectioned in 3–5 μm sections onto glass slides, and stained with hematoxylin and eosin (Richard Allen Scientific, ThermoFisher) following manufacturer's instructions. Histology images were taken using a Nikon Eclipse 80i microscope and adipocytes were quantified using ImageJ software. Images of SOST-Ab treated sections were captured by Scanscope CS2 and analyzed by Aperio Imagescope v11.2.0.780 to generate images for analysis. ImageJ length tool and cell count plugin was used to determine adipocyte number and average area of all adipocytes in 1 field of view (FOV) (image taken from 20X objective). Four FOVs per slide were taken and

averaged together to obtain an average adipocyte area per total area for each animal. Adipocyte area was calculated by calibrating each image based on the magnification of the microscope to a known distance using ImageJ. For the Nikon Eclipse 80i microscope at 20X objective this equated to 200 pixels per 400 μm.

Microcomputed Tomography and Osmium Tetroxide microCT

Micro-CT was performed on bones in PBS with an energy level of 55 kVp and intensity of 145 μA. The integration time was set to 500 ms at a maximum isometric voxel size of 10.5 μm at a high-resolution setting using a VivaCT-40 (Scanco Medical, Bruttisellen, Switzerland). Three VOI were selected: (1) the proximal tibia to the growth plate, (2) from the growth plate to the tibia/fibula junction, and (3) distal of the tibia/fibula junction. First, cortical bone was analyzed with a threshold of 280, the growth plates and tibia/fibula junction were identified and the distance in slices between the two calculated. A total for 30 slices were evaluated. Secondly, trabecular bone volume fraction and microarchitecture were evaluated below the growth plate. Approximately 230 consecutive slices were made at the distal end of the growth plate and extending in a proximal direction, and 180 contiguous slices were selected for analysis. The total volume of mouse bones was determined by contouring around the entire bone between the growth plate and tibia/fibula junction, and then calculating the bone volume and total volume using a threshold of 220.

Osmium staining for marrow adiposity analysis was performed in collaboration with the Small Animal Imaging Core and the Physiology Core at Maine Medical Center Research Institute following previously published methods (Scheller et al. 2014). Briefly tibias were isolated, fixed with 10% NBF for 24 hours, washed and then decalcified for 14 days in EDTA. Upon further washing bones were then stained for 48 hours in 1% osmium tetroxide. After subsequent washes, bones were then scanned in PBS with an energy level of 55kVp, and intensity of 145 μA. The integration time was set to 500 ms at a maximum isometric voxel size of 10. 5 μm at a high-resolution setting using a VivaCT-40 (Scanco Medical).

Oil Red O Staining

Cells were washed with phosphate buffered saline (PBS) and fixed with 4% NBF for 1 hour at 37°C. Cells were then rinsed with 60% isopropanol prior to a 30 minute Oil Red O (3.5 mg/mL, AMRESCO, Solon, OH) incubation. Oil Red O was then removed and followed by four additional PBS washes during which time cells were imaged for phenotypic assessment of lipid accumulation. Quantification of Oil Red O was performed by eluting the stain from the cells with 100% isopropanol and quantifying the absorbance at 490nm against an Oil Red O standard curve on a spectrophotometer (Modulus Microplate, Turner Biosystems).

mRNA Isolation and qRT-PCR

Total mRNA was isolated from cells using the miRNeasy isolation mini-kit (Qiagen, Hilden, Germany) according to the manufacturer's protocol. Total mRNA samples were quantified and tested for quality and contamination using a nanodrop machine (ThermoScientific) before cDNA synthesis (SuperScript III First Strand Synthesis, Life Sciences; Applied Biosciences High Capacity cDNA Kit, ThermoScientific, Waltham, MA) according to the manufacturer's instructions. qRT-PCR was performed using SYBR Master Mix (Bio-Rad,

Hercules, CA) and thermocycling reactions were completed using a CFX-384 (Bio-Rad). Data was analyzed using Bio-Rad CFX Manager 3.1 and Microsoft Excel. Statistics and graphs were generated using GraphPad Prism 6 software (Graphpad Software Inc., La Jolla, CA).

Sclerostin ELISA and Reagents

Cell culture media was collected from osteocytes following 2–3 days in culture and frozen at −20° C. To investigate the amount of SOST secreted into the media by primary osteocyte cells, a Mouse/Rat SOST/Sclerostin Quantikine kit was used (R&D Systems, Minneapolis, MN, USA). Recombinant mouse and human sclerostin were obtained from R&D Systems. Anti-sclerostin antibody and control buffer were provided by Novartis Pharma and Mereo Pharma.

Results

Recombinant SOST and Osteocyte-conditioned media containing SOST induce adipogenesis in 3T3-L1 pre-adipocytes

First, the well-characterized 3T3-L1 preadipocyte cell line was used to confirm previously reported effects of sclerostin on white pre-adipocytes (Ukita et al. 2016). Regulation of adipogenesis was evaluated by lipid accumulation and change in cell morphology during differentiation in the presence of recombinant sclerostin protein (rSOST). 3T3-L1 cells were grown in basal media or adipogenic induction regiment media with or without rSOST, which was added with each media change (0, 2, 5, and 7 days). We observed an increase in Oil Red O staining in these cells in the presence of 1 ng/mL sclerostin in basal media (Figure 1A, B). The expression of adipogenic transcription factors *Pparγ* and *Cebpβ* were also significantly increased in cells treated with rSOST (Figure 1C, D). Next, to determine if osteocyte-derived SOST could also induce adipogenesis in 3T3-L1 cells and to better understand effects of sclerostin secreted from osteocytes *in vivo*, we isolated primary mouse osteocytes and used these to create conditioned media (Ocy-CM). Using ELISA, we measured the amount of SOST protein secreted into the media and found that SOST levels were between 500–1000 pg/mL (Figure 1E), which is similar to the ranges observed in circulation in humans (0.84 – 1.27 ng/mL)(Ma et al. 2014). We assessed the effects of this conditioned media on 3T3-L1 and found that it significant increased 3T3-L1 adipogenesis as assessed by Oil Red O staining (Figure 1F).

SOST induces adipogenesis in ear mesenchymal stromal cells

To further investigate the effect of SOST on stromal cell differentiation using primary cells, we used primary mouse MSCs extracted from mouse external ear tissue samples (eMSCs). We found that eMSCs were also responsive to sclerostin treatment and observed an increase in Oil Red O accumulation after 7 days in adipogenic media supplemented with 10 ng/mL rSOST versus control (Figure 2A). These effects were mirrored in the gene expression data where *Pparγ* and *Cebpα* were both significantly upregulated in response to rSOST treatment (Figure 2B, C).

SOST protein and Osteocyte-conditioned media containing SOST induce adipogenesis in mouse primary BM-MSCs

To investigate the effects of sclerostin on bone marrow adipogenesis specifically, we isolated adherent BM-MSCs from murine tibia and femur, and tested their response to rSOST and Ocy-CM. Mouse BM-MSCs demonstrated increased adipogenesis in response rSOST as measured by Oil Red O accumulation (Figure 3A) and the expression of adipogenic transcription factors *Pparγ* (Figure 3B) and *Cebpα* (data not shown) measured by qRT-PCR, also were significantly increased in response to sclerostin. Importantly, these effects were accompanied by a significant decrease in the β-catenin-responsive gene Axin2 (Figure 3C), and a decrease, although not significant, in the β-catenin-responsive gene Smad6 (Figure 3D). These data suggest that increased adipogenesis in response to SOST treatment occurs via inhibition of the canonical WNT signaling pathway. Moreover, Ocy-CM also significantly increased Oil Red O staining (Figure 3E) and *Cebpα* gene expression (Figure 3F). Although *Pparγ* expression was also increased by Ocy-CM, this result was not significant (Figure 3G), while Adiponectin (*Adipoq*), expressed in mature adipocytes, was significantly upregulated with Ocy-CM treatment (Figure 3H). These findings suggest that media derived from osteocytes containing 0.5–1 μg/mL sclerostin can increase adipogenesis in preadipocytes and primary mouse BM-MSCs.

Significant increases in adipogenesis were also observed in MSCs derived from human patient samples with rSost treatment as quantified by Oil Red O staining and quantification (Supplemental Figure 1). SOST trended towards increasing human BM-MSC *PPARγ* expression, but significant gene expression changes was not observed in ($p=0.087$, data not show).

Loss of SOST in mice reduces BMAT in *in vivo* genetic knockout and antibody treatment models

Based on the consistent positive effects of sclerostin on adipogenesis *in vitro*, we chose to examine the effect of sclerostin on BMAT *in vivo*. Sclerostin knock-out (SOST-KO) and wild type (WT) control mice were sacrificed at 6-weeks of age and long bones were collected and fixed in formalin prior to analysis for bone parameters and BMAT accumulation. Representative images of H&E are found in Figure 4A (WT) and Figure 4B (Sost-KO). Consistent with previous reports, we observed and quantified statistically significant increases in trabecular bone volume/total volume (BV/TV) (Figure 4C) and cortical thickness (Figure 4D) in SOST-KO vs WT mice. Cortical porosity was also decreased in SOST-KO animals (Figure 4E). Osmium tetroxide (OsO_4) staining and OsO_4 μCT analysis demonstrated significantly lower levels of BMAT accumulation (mm^3) in SOST-KO tibias compared to WT controls in both proximal (Figure 4F) and distal (Figure 4G) locations.

In a second model of decreased SOST signaling, wild-type mice were treated with sclerostin neutralizing antibody (Anti-SOST Ab) at 100 mg/kg i.v. weekly or vehicle, and decreased BMAT was observed after Anti-SOST Ab treatment (Figure 5). In rodents, this dosage has been confirmed to significantly increase proximal tibia BV/TV (%), and femoral strength, cortical thickness, and cross-sectional moment of inertia (Moe et al. 2015). Anti-SOST Ab

treatment led to significantly fewer adipocytes in the BM compartment (Figure 5A and B) as well as significantly smaller adipocyte number (Figure 5C) and size (Figure 5D).

Discussion

Adipose tissue is now widely considered to be an endocrine organ that engages in cellular cross-talk with the brain as well as other peripheral tissue types. A better understanding of adipose development and regulation would greatly enhance our ability to fight numerous diseases. BMAT is a more recently characterized, unique depot that is now recognized as a key player in diseases of the marrow (Scheller & Rosen 2014). However, the relationship between the marrow adipose depot and osteocytes or osteocyte-derived molecules, such as sclerostin, has as yet been unexplored. In this study we show that osteocyte-derived factors enhance adipocyte differentiation, not only in pre-adipocyte cell lines, but also in primary MSCs from mouse and human. These *in vitro* experiments with both osteocyte-conditioned media as well as direct addition of recombinant sclerostin demonstrate that treatment with SOST causes the upregulation of critical adipogenic transcription factors *Pparγ* and *Cebpβ* and increases lipid accumulation. We also examined a potential effect of SOST in ear MSCs (eMSCs) which have been shown to differentiate into adipocytes *in vitro*. Importantly, we saw a consistent positive response to recombinant SOST treatment in these cells, indicating that multipotent primary cells are responsive to sclerostin.

Very little is known about the interaction between SOST and BM stromal cells *in vivo*. In our work, two *in vivo* models of SOST inhibition confirmed that BMAT is induced by SOST and decreased upon SOST knockout or neutralization with a neutralizing antibody. In accordance with previous reports (Morse et al. 2015; Li et al. 2008), we observed an increase in bone mineral density, cortical thickness, and trabecular thickness in SOST-KO mice. Importantly, we examined the BM adipose profiles in these animals and found significantly reduced BMAT, indicating an inverse relationship between bone and BMAT, and suggesting that SOST itself modulates BMAT *in vivo*. To further test this hypothesis, we injected mice with a SOST neutralizing antibody and saw a decrease in the number of marrow adipocytes as well as a decrease in adipocyte size in the mice treated with the antibody. These data support the idea that SOST signaling via osteocytes is part of a tight regulatory network within the marrow cavity and further suggest that changes in this network—either due to aging or disease—can skew the ratio of BM cell types (Figure 6).

The Wnt signaling influences on BM adipogenesis we observed are consistent with other findings (Kennell & MacDougald 2005; Qiu et al. 2007). Our data are also consistent with data from other models that found a significant decrease in adipocyte within the fracture callus in mice treated with anti-sclerostin antibodies versus controls in a diabetic streptozotocin mouse fracture model (Yee et al. 2016). However, these authors found no significant difference in healthy controls treated with anti-sclerostin antibodies perhaps because they used half the antibody dose that we used here. Additionally, we used a different route of administration and different mouse backgrounds.

Our data are also consistent with observed clinical correlations. For example, in men it has been observed that circulating sclerostin levels correlate with increased abdominal

subcutaneous and visceral adipose, total fat by DXA, and BM adipose content in the vertebrae, even when adjusted for age, diabetes status and BMI (Ma et al. 2014). Sclerostin increases with age in humans, which correlates with decreases in bone formation and increases in BM adiposity (Kügel et al. 2001; Griffith et al. 2005). Circulating sclerostin has also been linked to systemic adiposity (Amrein et al. 2012; Urano et al. 2012; Ma et al. 2014). While this effect is consistent in men, the results are less clear in women and suggest a sex difference that should be explored in future studies. Other clinical data found that high vertebral BMAT is correlated with either increased or decreased in bone, in both osteoporotic patients and patients with anorexia respectively, (Griffith et al. 2005), suggesting that this adipose depot is both regulated by bone signals and dynamically responsive to disease. Indeed, SOST dysregulation has been linked to bone-metastasizing cancers, making it a therapeutically relevant target that may play a role in cancer (Morris & Edwards 2016) not only as an osteoblast inhibitor, but also potentially via the activation of BM adipogenesis. Thus, sclerostin may be playing a part of the vicious cycle in bone metastasis through its effects on BMAT, a concept that has not been previously recognized.

Our work has expanded the known regulatory sphere of osteocyte influence. These findings indicate that osteocyte- and osteocyte-factor targeted therapies, such as anti-DKK1 and anti-Sclerostin antibodies, may influence not only osteoclasts and osteoblasts, but also BM adipocytes, which suggests secondary modes of action for bone anabolic therapeutics that had not been previously appreciated. The osteocyte thus plays an even more essential role in controling bone than previously understood. Sclerostin as a BMAT inducer can now be added to the list of soluble factors that have been shown to increase BMAT, including rosiglitazone (which increased BMAT and decreases visceral WAT (de Paula et al. 2015)), high fat diets (Styner et al. 2014; Doucette et al. 2015), aging (Takeshita et al. 2014), and caloric restriction (Devlin et al. 2010). Future directions should be targeted at understanding why BMAT arises in certain states, and whether this results from sclerostin secretion or other mechanisms (e.g., a loss of hematopoiesis due to the negative energy balance during starvation or increased adipogenesis resulting from the need to store calories in the net positive energy state of obesity) (Devlin 2011). Other ongoing work will determine the roles of BMAT in skeletal metabolism and bone tissue modeling and remodeling, especially due to the frequent observations of an inverse correlation between BMAT and bone mineral density in children and adults (Shen et al. 2007; Shen et al. 2012; Shen et al. 2014). Further characterization of the phenotype and the functional regulation of BMAT is also needed (Hardouin et al. 2016). The difficulties in accessing BMAT currently hamper researchers' abilities to elucidate the contribution of BMAT, relative to contributions from peripheral adipose tissues, to many pathologies. Thus, other future directions include development of better *in vivo* and *ex vivo* models of BMAT to study this unique depot. Such models could help scientists understand the relationship between bone and fat cells and help identify other lineage switch molecules, similar to sclerostin, which could also be targeted to have a clinical impact on age-related osteoporosis, diabetes, and obesity. Overall, this study demonstrates a direct tie between SOST and BMAT, adding another layer of complexity to any correlation of SOST with disease phenotypes. Our work underscores the importance of continued investigation into the bone-BMAT relationship and regulation of the BM. In sum,

our work adds to the field by identifying a soluble, targetable factor that has the potential to be used clinically to modulate BM adipogenesis.

Supplementary Material

Refer to Web version on PubMed Central for supplementary material.

Acknowledgments

Funding: National Institute of General Medical Sciences through a pilot project and the histology and physiology core from NIH P30 GM106391, Phase III COBRE in Progenitor Cells (D. Wojchowski P.I.) and support from NIH P30GM103392, Phase III COBRE in Vascular Biology (R. Friesel, P.I.). The authors' work is supported by start-up funds from the Maine Medical Center Research Institute and the NIH/NIDDK (R24 DK092759-01).

The authors' work is supported by MMCRI start-up funds, a pilot project grant from NIH/NIGMS (P30GM106391), and the NIH/NIDDK (R24DK092759-01). We thank Dr. David Maridas, Dr. Anyonya Guntar, Phuong Le, Sheila Bornstein, and Carolina Figueroa for help with protocol optimization, sharing reagents and scientific discussions for this work. We thank Novartis Pharma, Basel Switzerland, and Mereo Pharma, UK for supply of anti-sclerostin antibody and vehicle buffer.

References

Almeida M, Han L, Bellido T, Manolagas SC, Kousteni S. Wnt proteins prevent apoptosis of both uncommitted osteoblast progenitors and differentiated osteoblasts by beta-catenin-dependent and -independent signaling cascades involving Src/ERK and phosphatidylinositol 3-kinase/AKT. The Journal of biological chemistry. 2005; 280(50):41342–51. [PubMed: 16251184]

Amrein K, Amrein S, Drexler C, Dimai HP, Dobnig H, Pfeifer K, Tomaschitz A, Pieber TR, Fahrleitner-Pammer A. Sclerostin and its association with physical activity, age, gender, body composition, and bone mineral content in healthy adults. The Journal of clinical endocrinology and metabolism. 2012; 97(1):148–54. [PubMed: 21994959]

Costa AG, Bilezikian JP, Lewiecki EM. Update on romosozumab: a humanized monoclonal antibody to sclerostin. Expert opinion on biological therapy. 2014; 14(5):697–707. [PubMed: 24665957]

Devlin MJ. Why does starvation make bones fat? American Journal of Human Biology. 2011; 23(5): 577–585. [PubMed: 21793093]

Devlin MJ, Cloutier AM, Thomas NA, Panus DA, Lotinun S, Pinz I, Baron R, Rosen CJ, Bouxsein ML. Caloric restriction leads to high marrow adiposity and low bone mass in growing mice. Journal of bone and mineral research: the official journal of the American Society for Bone and Mineral Research. 2010; 25(9):2078–88.

van Dinther M, Zhang J, Weidauer SE, Boschert V, Muth E-M, Knappik A, de Gorter DJJ, van Kasteren PB, Frisch C, Mueller TD, ten Dijke P. Anti-Sclerostin antibody inhibits internalization of Sclerostin and Sclerostin-mediated antagonism of Wnt/LRP6 signaling. PloS one. 2013; 8(4):e62295. [PubMed: 23638027]

Doucette CR, Horowitz MC, Berry R, MacDougald OA, Anunciado-Koza R, Koza RA, Rosen CJ. A High Fat Diet Increases Bone Marrow Adipose Tissue (MAT) But Does Not Alter Trabecular or Cortical Bone Mass in C57BL/6J Mice. Journal of cellular physiology. 2015; 230(9):2032–7. [PubMed: 25663195]

Falank C, Fairfield H, Reagan MR. Signaling Interplay between Bone Marrow Adipose Tissue and Multiple Myeloma cells. Frontiers in endocrinology. 2016; 7:67. [PubMed: 27379019]

Fan Y, Hanai J, Le PT, Bi R, Maridas D, DeMambro V, Figueroa CA, Kir S, Zhou X, Mannstadt M, Baron R, Bronson RT, Horowitz MC, Wu JY, Bilezikian JP, Dempster DW, Rosen CJ, Lanske B. Parathyroid Hormone Directs Bone Marrow Mesenchymal Cell Fate. Cell Metabolism. 2017 Epub ahead of print.

Florio M, Gunasekaran K, Stolina M, Li X, Liu L, Tipton B, Salimi-Moosavi H, Asuncion FJ, Li C, Sun B, Tan HL, Zhang L, Han C-Y, Case R, Duguay AN, Grisanti M, Stevens J, Pretorius JK,

Pacheco E, et al. A bispecific antibody targeting sclerostin and DKK-1 promotes bone mass accrual and fracture repair. Nature communications. 2016; 7:11505.

Fulzele K, Riddle RC, DiGirolamo DJ, Cao X, Wan C, Chen D, Faugere M-C, Aja S, Hussain MA, Brüning JC, Clemens TL. Insulin receptor signaling in osteoblasts regulates postnatal bone acquisition and body composition. Cell. 2010; 142(2):309–19. [PubMed: 20655471]

Genant HK, Engelke K, Bolognese MA, Mautalen C, Brown JP, Recknor C, Goemaere S, Fuerst T, Yang Y-C, Grauer A, Libanati C. Effects of Romosozumab Compared With Teriparatide on Bone Density and Mass at the Spine and Hip in Postmenopausal Women With Low Bone Mass. Journal of bone and mineral research: the official journal of the American Society for Bone and Mineral Research. 2017; 32(1):181–187.

Griffith JF, Yeung DKW, Antonio GE, Lee FKH, Hong AWL, Wong SYS, Lau EMC, Leung PC. Vertebral bone mineral density, marrow perfusion, and fat content in healthy men and men with osteoporosis: dynamic contrast-enhanced MR imaging and MR spectroscopy. Radiology. 2005; 236(3):945–51. [PubMed: 16055699]

Gustafson B, Smith U. The WNT inhibitor Dickkopf 1 and bone morphogenetic protein 4 rescue adipogenesis in hypertrophic obesity in humans. Diabetes. 2012; 61(5):1217–24. [PubMed: 22447857]

Hardouin P, Rharass T, Lucas S. Bone Marrow Adipose Tissue: To Be or Not To Be a Typical Adipose Tissue? Frontiers in endocrinology. 2016; 7:85. [PubMed: 27445987]

Heath DJ, Chantry AD, Buckle CH, Coulton L, Shaughnessy JD, Evans HR, Snowden JA, Stover DR, Vanderkerken K, Croucher PI. Inhibiting Dickkopf-1 (Dkk1) removes suppression of bone formation and prevents the development of osteolytic bone disease in multiple myeloma. Journal of bone and mineral research: the official journal of the American Society for Bone and Mineral Research. 2009; 24(3):425–36.

Keller H, Kneissel M. SOST is a target gene for PTH in bone. Bone. 2005; 37(2):148–58. [PubMed: 15946907]

Kennell JA, MacDougald OA. Wnt signaling inhibits adipogenesis through beta-catenin-dependent and -independent mechanisms. The Journal of biological chemistry. 2005; 280(25):24004–10. [PubMed: 15849360]

Kim SW, Lu Y, Williams EA, Lai F, Lee JY, Enishi T, Balani DH, Ominsky MS, Ke HZ, Kronenberg HM, Wein MN. Sclerostin Antibody Administration Converts Bone Lining Cells Into Active Osteoblasts. Journal of Bone and Mineral Research. 2016

Kügel H, Jung C, Schulte O, Heindel W. Age-and sex-specific differences in the 1 H-spectrum of vertebral bone marrow. Journal of magnetic resonance imaging: JMRI. 2001; 268:263–268.

Li C, Ominsky MS, Tan H-L, Barrero M, Niu Q-T, Asuncion FJ, Lee E, Liu M, Simonet WS, Paszty C, Ke HZ. Increased callus mass and enhanced strength during fracture healing in mice lacking the sclerostin gene. Bone. 2011; 49(6):1178–85. [PubMed: 21890008]

Li X, Niu Q-T, Warmington KS, Asuncion FJ, Dwyer D, Grisanti M, Han C-Y, Stolina M, Eschenberg MJ, Kostenuik PJ, Simonet WS, Ominsky MS, Ke HZ. Progressive increases in bone mass and bone strength in an ovariectomized rat model of osteoporosis after 26 weeks of treatment with a sclerostin antibody. Endocrinology. 2014; 155(12):4785–97. [PubMed: 25259718]

Li X, Ominsky MS, Niu Q-T, Sun N, Daugherty B, D'Agostin D, Kurahara C, Gao Y, Cao J, Gong J, Asuncion F, Barrero M, Warmington K, Dwyer D, Stolina M, Morony S, Sarosi I, Kostenuik PJ, Lacey DL, et al. Targeted deletion of the sclerostin gene in mice results in increased bone formation and bone strength. Journal of Bone and Mineral Research. 2008; 23(6):860–9. [PubMed: 18269310]

Liaw L, Prudovsky I, Koza RA, Anunciado-Koza RV, Siviski ME, Lindner V, Friesel RE, Rosen CJ, Baker PRS, Simons B, Vary CPH. Lipid Profiling of In Vitro Cell Models of Adipogenic Differentiation: Relationships With Mouse Adipose Tissues. Journal of cellular biochemistry. 2016; 117(9):2182–93. [PubMed: 26910604]

Ma Y-HV, Schwartz AV, Sigurdsson S, Hue TF, Lang TF, Harris TB, Rosen CJ, Vittinghoff E, Eiriksdottir G, Hauksdottir AM, Siggeirsdottir K, Sigurdsson G, Oskarsdottir D, Napoli N, Palermo L, Gudnason V, Li X. Circulating sclerostin associated with vertebral bone marrow fat in older men but not women. The Journal of clinical endocrinology and metabolism. 2014; 99(12):E2584–90. [PubMed: 25144629]

McClung MR, Grauer A, Boonen S, Bolognese MA, Brown JP, Diez-Perez A, Langdahl BL, Reginster J-Y, Zanchetta JR, Wasserman SM, Katz L, Maddox J, Yang Y-C, Libanati C, Bone HG. Romosozumab in postmenopausal women with low bone mineral density. The New England journal of medicine. 2014; 370(5):412–20. [PubMed: 24382002]

Moe SM, Chen NX, Newman CL, Organ JM, Kneissel M, Kramer I, Gattone VH, Allen MR. Anti-Sclerostin Antibody Treatment in a Rat Model of Progressive Renal Osteodystrophy. Journal of Bone and Mineral Research. 2015; 30(3):499–509. [PubMed: 25407607]

Morris EV, Edwards CM. Bone Marrow Adipose Tissue: A New Player in Cancer Metastasis to Bone. Frontiers in endocrinology. 2016; 7:90. [PubMed: 27471491]

Morrison RF, Farmer SR. Role of PPARgamma in regulating a cascade expression of cyclin-dependent kinase inhibitors, p18(INK4c) and p21(Waf1/Cip1), during adipogenesis. The Journal of biological chemistry. 1999; 274(24):17088–97. [PubMed: 10358062]

Morse A, Yu NYC, Peacock L, Mikulec K, Kramer I, Kneissel M, McDonald MM, Little DG. Endochondral fracture healing with external fixation in the Sost knockout mouse results in earlier fibrocartilage callus removal and increased bone volume fraction and strength. Bone. 2015; 71:155–63. [PubMed: 25445453]

Mosialou I, Shikhel S, Liu J-M, Maurizi A, Luo N, He Z, Huang Y, Zong H, Friedman RA, Barasch J, Lanzano P, Deng L, Leibel RL, Rubin M, Nicholas T, Chung W, Zeltser LM, Williams KW, Pessin JE, et al. MC4R-dependent suppression of appetite by bone-derived lipocalin 2. Nature. 2017; 543(7645):385–390. [PubMed: 28273060]

Ominsky MS, Boyce RW, Li X, Ke HZ. Effects of sclerostin antibodies in animal models of osteoporosis. Bone. 2017; 96:63–75. [PubMed: 27789417]

de Paula FJA, de Araújo IM, Carvalho AL, Elias J, Salmon CEG, Nogueira-Barbosa MH. The Relationship of Fat Distribution and Insulin Resistance with Lumbar Spine Bone Mass in Women. PloS one. 2015; 10(6):e0129764. [PubMed: 26067489]

Qiu W, Andersen TE, Bollerslev J, Mandrup S, Abdallah BM, Kassem M. Patients with high bone mass phenotype exhibit enhanced osteoblast differentiation and inhibition of adipogenesis of human mesenchymal stem cells. Journal of bone and mineral research: the official journal of the American Society for Bone and Mineral Research. 2007; 22(11):1720–31.

Reagan MR, Mishima Y, Glavey SV, Zhang YY, Manier S, Lu ZN, Memarzadeh M, Zhang YY, Sacco A, Aljawai Y, Shi J, Tai Y, John E, Kaplan DL, Roccaro AM, Ghobrial IM, Ready JE, Kaplan DL, Roccaro AM, et al. Investigating osteogenic differentiation in multiple myeloma using a novel 3D bone marrow niche model. Blood. 2014; 124(22):3250–9. [PubMed: 25205118]

Roschger A, Roschger P, Keplingter P, Klaushofer K, Abdullah S, Kneissel M, Rauch F. Effect of sclerostin antibody treatment in a mouse model of severe osteogenesis imperfecta. Bone. 2014; 66:182–8. [PubMed: 24953712]

Saini V, Marengi DA, Barry KJ, Fulzele KS, Heiden E, Liu X, Dedic C, Maeda A, Lotinun S, Baron R, Pajevic PD. Parathyroid hormone (PTH)/PTH-related peptide type 1 receptor (PPR) signaling in osteocytes regulates anabolic and catabolic skeletal responses to PTH. The Journal of biological chemistry. 2013; 288(28):20122–34. [PubMed: 23729679]

Schaffler MB, Cheung W-Y, Majeska R, Kennedy O. Osteocytes: master orchestrators of bone. Calcified tissue international. 2014; 94(1):5–24. [PubMed: 24042263]

Scheller EL, Rosen. What's the matter with MAT? Marrow adipose tissue, metabolism, and skeletal health. Annals of the New York Academy of Sciences. 2014; 1311:14–30. [PubMed: 24650218]

Scheller EL, Troiano N, Vanhoutan JN, Bouxsein MA, Fretz JA, Xi Y, Nelson T, Katz G, Berry R, Church CD, Doucette CR, Rodeheffer MS, Macdougald OA, Rosen CJ, Horowitz MC. Use of osmium tetroxide staining with microcomputerized tomography to visualize and quantify bone marrow adipose tissue in vivo. Methods in enzymology. 2014; 537:123–39. [PubMed: 24480344]

Schutze N, Noth U, Schneidereit J, Hendrich C, Jakob F. Differential expression of CCN-family members in primary human bone marrow-derived mesenchymal stem cells during osteogenic, chondrogenic and adipogenic differentiation. Cell communication and signaling. 2005; 3(1):5. [PubMed: 15773998]

Shen W, Chen J, Punyanitya M, Shapses S, Heshka S, Heymsfield SB. MRI-measured bone marrow adipose tissue is inversely related to DXA-measured bone mineral in Caucasian women.

Osteoporosis international: a journal established as result of cooperation between the European Foundation for Osteoporosis and the National Osteoporosis Foundation of the USA. 2007; 18(5): 641–7.

Shen W, Scherzer R, Gantz M, Chen J, Punyanitya M, Lewis CE, Grunfeld C. Relationship between MRI-measured bone marrow adipose tissue and hip and spine bone mineral density in African-American and Caucasian participants: the CARDIA study. The Journal of clinical endocrinology and metabolism. 2012; 97(4):1337–46. [PubMed: 22319043]

Shen W, Velasquez G, Chen J, Jin Y, Heymsfield SB, Gallagher D, Pi-Sunyer FX. Comparison of the relationship between bone marrow adipose tissue and volumetric bone mineral density in children and adults. Journal of clinical densitometry. 2014; 17(1):163–9. [PubMed: 23522982]

Singh L, Brennan TA, Russell E, Kim J-H, Chen Q, Brad Johnson F, Pignolo RJ. Aging alters bone-fat reciprocity by shifting in vivo mesenchymal precursor cell fate towards an adipogenic lineage. Bone. 2016; 85:29–36. [PubMed: 26805026]

Stern AR, Stern MM, Van Dyke ME, Jähn K, Prideaux M, Bonewald LF, Rath Stern A, Stern MM, Van Dyke ME, Jähn K, Prideaux M, Bonewald LF. Isolation and culture of primary osteocytes from the long bones of skeletally mature and aged mice. BioTechniques. 2012; 52(6):361–73. [PubMed: 22668415]

Styner M, Thompson WR, Galior K, Uzer G, Wu X, Kadari S, Case N, Xie Z, Sen B, Romaine A, Pagnotti GM, Rubin CT, Styner MA, Horowitz MC, Rubin J. Bone marrow fat accumulation accelerated by high fat diet is suppressed by exercise. Bone. 2014; 64:39–46. [PubMed: 24709686]

Takeshita S, Fumoto T, Naoe Y, Ikeda K. Age-related marrow adipogenesis is linked to increased expression of RANKL. The Journal of biological chemistry. 2014; 289(24):16699–710. [PubMed: 24753250]

Tian X, Jee WSS, Li X, Paszty C, Ke HZ. Sclerostin antibody increases bone mass by stimulating bone formation and inhibiting bone resorption in a hindlimb-immobilization rat model. Bone. 2011; 48(2):197–201. [PubMed: 20850580]

Tu X, Rhee Y, Condon KW, Bivi N, Allen MR, Dwyer D, Stolina M, Turner CH, Robling AG, Plotkin LI, Bellido T. Sost downregulation and local Wnt signaling are required for the osteogenic response to mechanical loading. Bone. 2012; 50(1):209–17. [PubMed: 22075208]

Ukita M, Yamaguchi T, Ohata N, Tamura M. Sclerostin Enhances Adipocyte Differentiation in 3T3-L1 Cells. Journal of Cellular Biochemistry. 2016; 117(6):1419–1428. [PubMed: 26553151]

Urano T, Shiraki M, Ouchi Y, Inoue S. Association of circulating sclerostin levels with fat mass and metabolic disease--related markers in Japanese postmenopausal women. The Journal of clinical endocrinology and metabolism. 2012; 97(8):E1473–7. [PubMed: 22639287]

Urs S, Venkatesh D, Tang Y, Henderson T, Yang X, Friesel RE, Rosen CJ, Liaw L. Sprouty1 is a critical regulatory switch of mesenchymal stem cell lineage allocation. FASEB journal: official publication of the Federation of American Societies for Experimental Biology. 2010; 24(9):3264–73. [PubMed: 20410440]

Yee CS, Xie L, Hatsell S, Hum N, Murugesh D, Economides AN, Loots GG, Collette NM. Sclerostin antibody treatment improves fracture outcomes in a Type I diabetic mouse model. Bone. 2016; 82:122–34. [PubMed: 25952969]

Yoshikawa Y, Kode A, Xu L, Mosialou I, Silva BC, Ferron M, Clemens TL, Economides AN, Kousteni S. Genetic evidence points to an osteocalcin-independent influence of osteoblasts on energy metabolism. Journal of Bone and Mineral Research. 2011; 26(9):2012–25. [PubMed: 21557308]

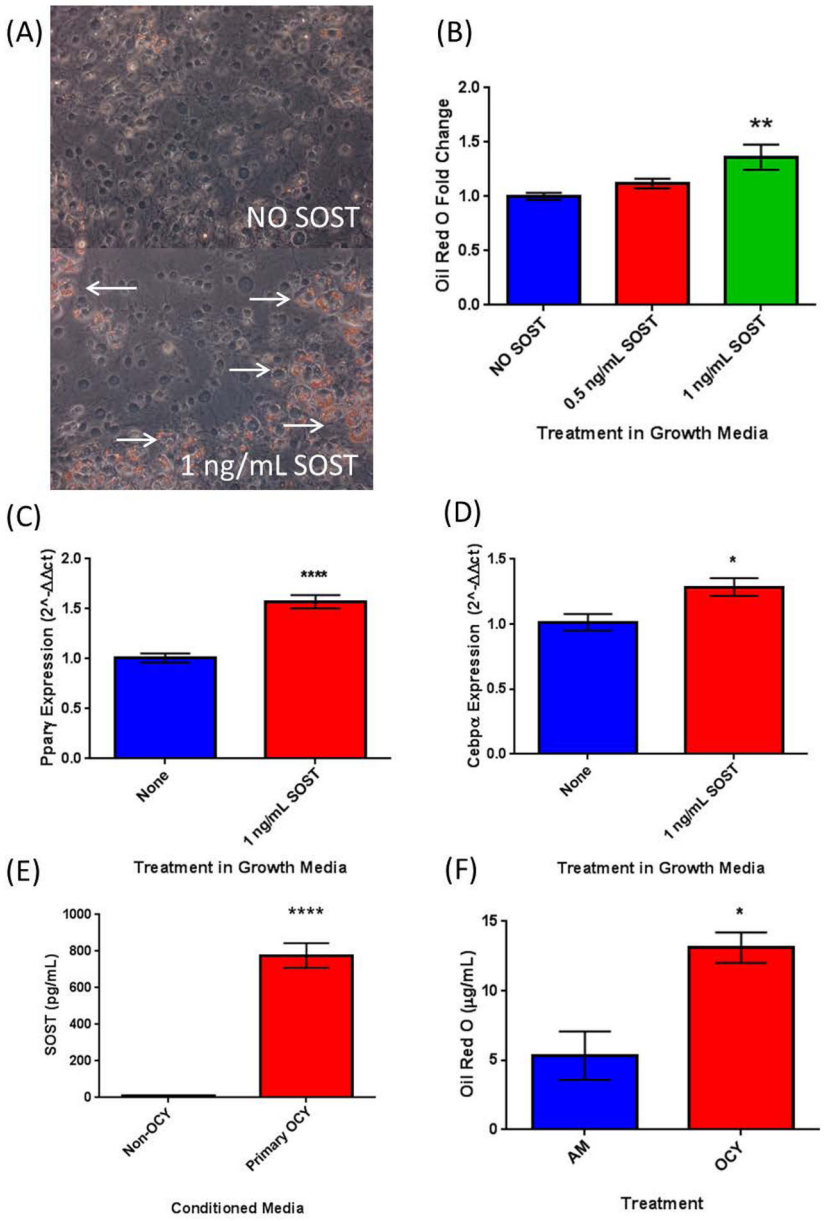

Figure 1.

3T3-L1 Cells. (A) Growth Media- Oil Red O Images; Top- Growth Media Alone, Bottom- Growth Media + 1ng/mL SOST and quantification. Arrows indicate Oil Red O staining. (B) Quantification of Oil Red O staining from A. (C) The upregulation of adipogenic transcription factor *Pparγ* and (D) *Cebpα* in response to SOST in basal growth media. (F) 3T3-L1 adipogenesis as measured via lipid accumulation is significantly upregulated in a 50/50 mixture of adipogenic media and media conditioned by primary mouse osteocytes, which produce high levels of sclerostin (E) as measured via ELISA.

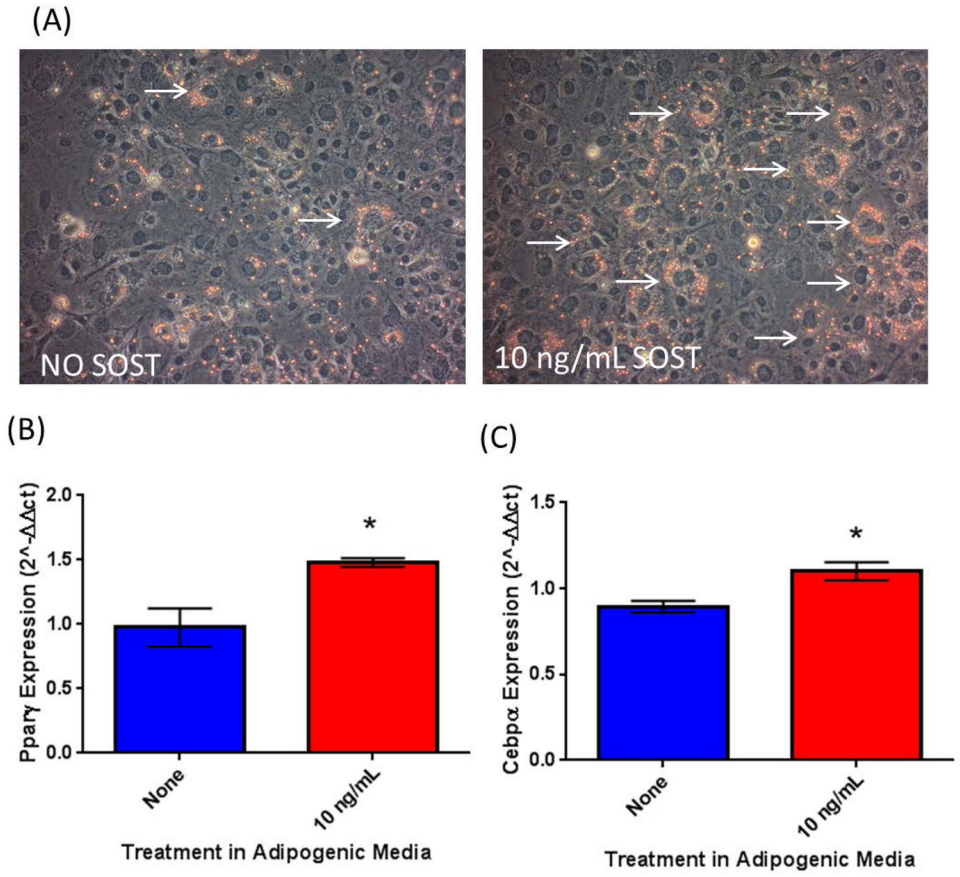

Figure 2.

SOST is able to induce adipogenesis in primary stem-like progenitors. Recombinant mouse sclerostin may induce lipid accumulation in ear mesenchymal stromal cells (eMSCs) (A). 10 ng/mL SOST induced an increase in adipogenic transcription factors *Pparg* (B) and *Cebpa* (C) after 7 days of differentiation.

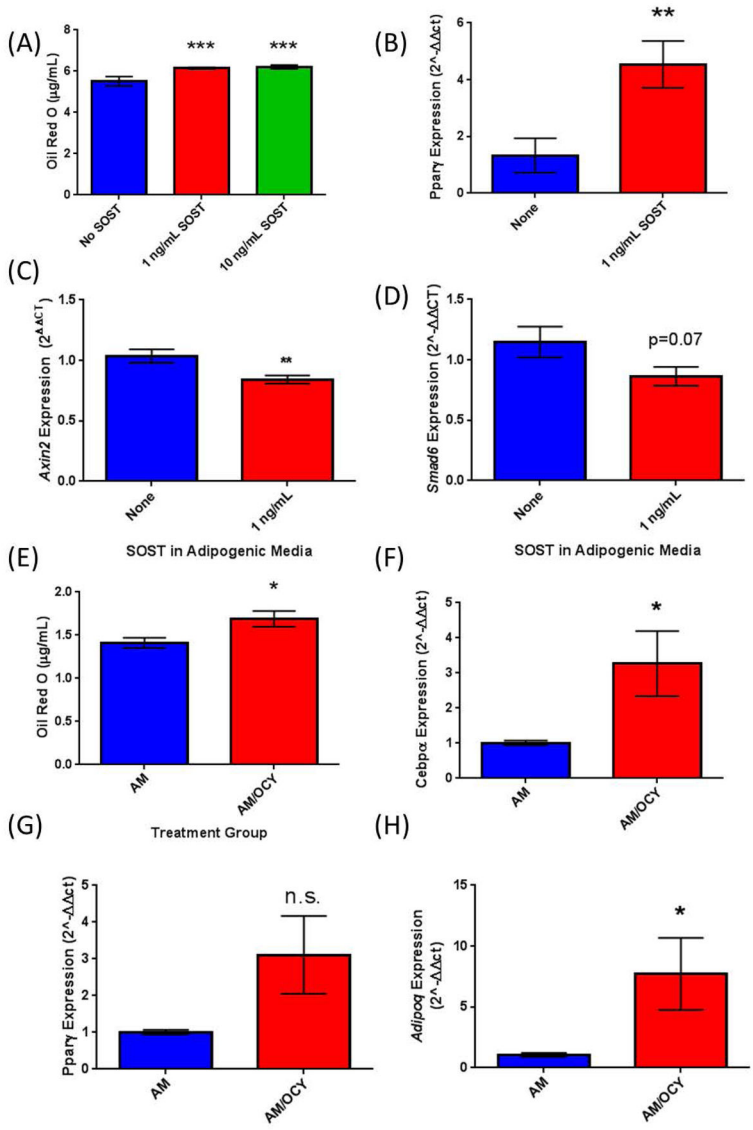

Figure 3.

Effects of Sost on BM-MSCs from Mouse. (A) Quantification of Oil Red O in BM-MSCs and upregulation of adipogenic transcription factors with SOST treatment. (B) BM-MSCs also showed an upregulation of adipogenic transcription factor Pparγ when treated with 1 ng/mL SOST. (C, D) β-catenin responsive genes *Axin2* and *Smad6* (H; n.s.) were decreased in response to SOST treatment in mouse BM-MSCs (E) Conditioned media from osteocytes induced elevated lipid accumulation in BM-MSCs as quantified by Oil Red O and induced an upregulation of adipogenic transcription factors *Cebpa* (F) and *Pparg* (G; n.s.). (H) The mature adipocyte marker adiponectin was also significantly increased in BM-MSCs exposed to osteocyte CM.

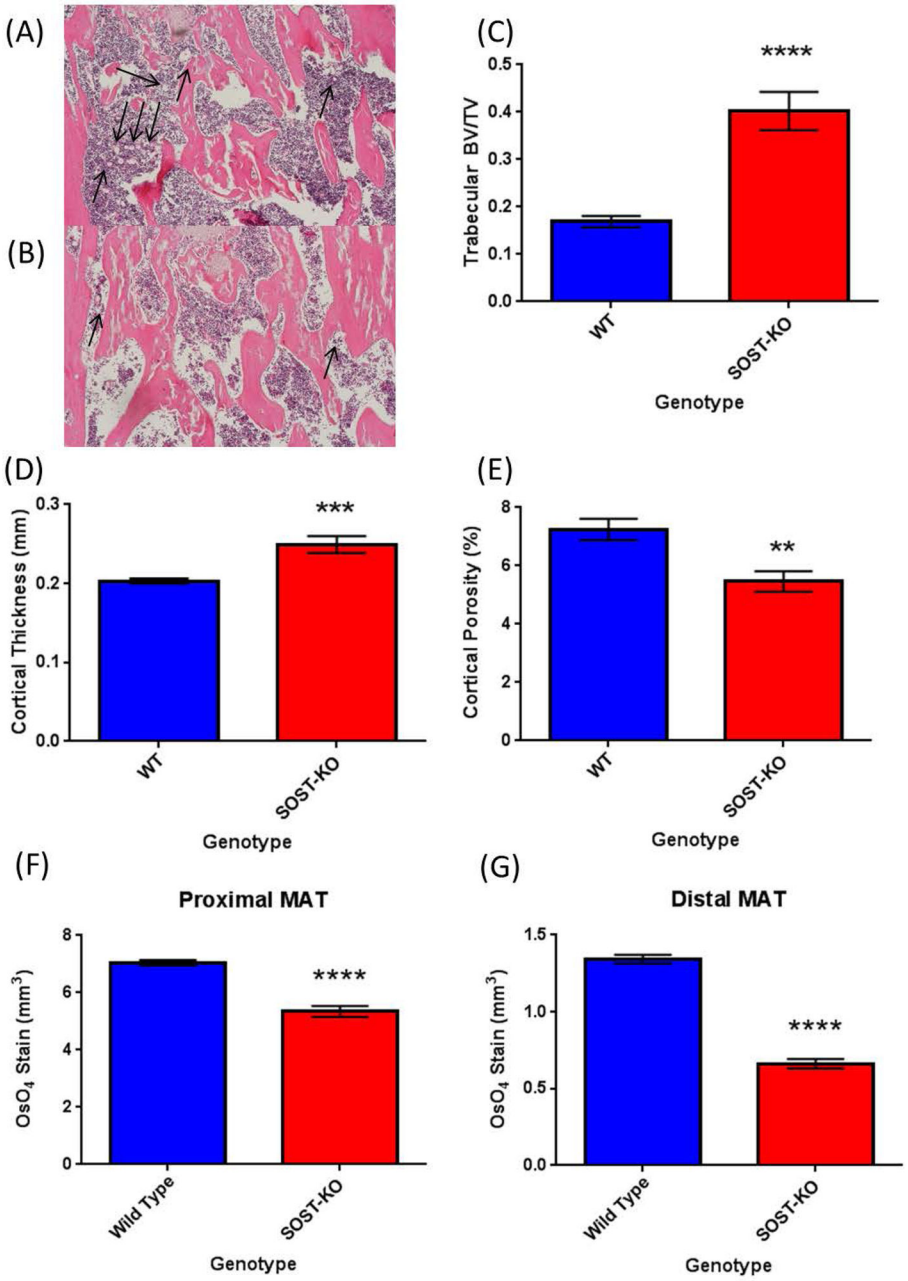

Figure 4.

Sclerostin knockout mice have altered bone and BMAT. (A) Bone marrow adipocytes are indicated by arrows in wild-type and (B) KO/KO animals; H&E stained sections of mouse femur. SOST-KO animals (males, 5–6 weeks of age; n=7) have higher bone parameters including trabecular bone volume/total volume (C), cortical thickness (D) and reduced cortical porosity (E) when compared to wild-type mice (n=8). SOST-KO mice have significantly lower marrow adipose tissue in both proximal (F) and distal (G) regions of the tibia as measured by osmium tetroxide μCT.

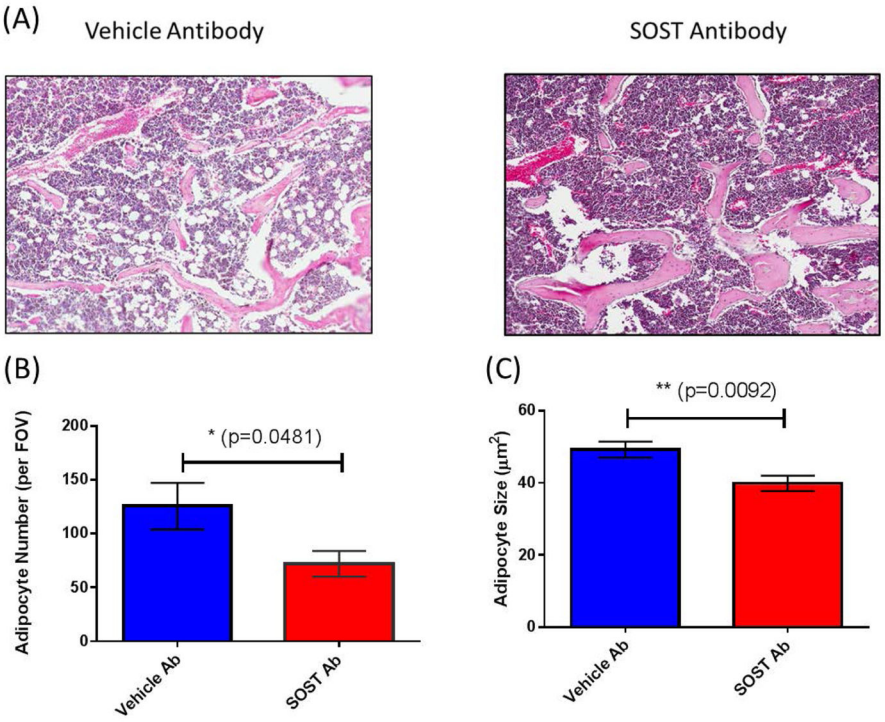

Figure 5.

Anti-Sclerostin antibody reduces BMAT *in vivo* (A & C); (A) H&E images and (B and C) quantification; * indicates significance via ANOVA. (D) Proposed model of sclerostin effects as an MSC fate switch determinant between adipogenesis and osteogenesis.

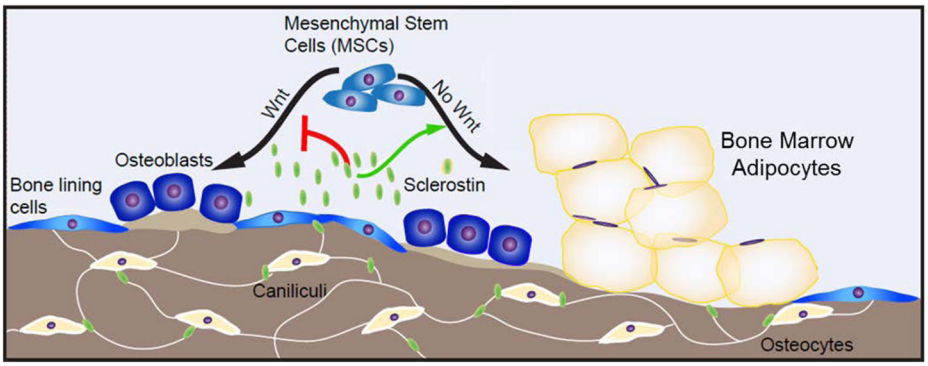

Figure 6.

Proposed model of sclerostin as an MSC fate switch determinant between adipogenesis and osteogenesis in the bone. Sclerostin, a gene that encodes the SOST protein, is expressed by osteocytes within cortical and trabecular bone. SOST protein is released from osteocytes and can regulate bone marrow progenitor cell differentiation by not only inhibiting osteogenesis, but also inducing adipogenesis. This novel role for sclerostin suggests that sclerostin-targeting therapies may not only increase osteogenesis, but also decrease bone marrow adipogenesis. In sum, our data reveal a previously undocumented role for sclerostin in development of bone marrow adipose.

Table 1

Primers used for qPCR.

Target	Forward	Reverse
Actb	CTCTGGCTCCTAGCACCATGAAGA	GTAAAACGCAGCTCAGTAACAGTCCG
Pparg	GCCCACCAACTTCGGAATC	TGCGAGTGGTCTTCCATCAC
Cebpa	TGGACAAGAACAGCAACGAG	TCACTGGTCAACTCCAGCAC
Adipoq	TGTTCCTCTTAATCCTGCCCA	CCAACCTGCACAAGTTCCCTT
Axin2	AAAACGGATTCAGGTCCTTCAA	GTCAGTGCGTCGCTGGATAAC
Smad6	GCGCGAGCTCCCTCATGTT	ACCTGAACATACGATACCCTT